How to cite: *Angew. Chem. Int. Ed.* **2025**, *64*, e202511186
doi.org/10.1002/anie.202511186

Analytical Chemistry

SPLICEIT Fluorescent Sensor for Integrating Dopamine Release with Cellular Resolution

*Steven M. Havens, Brian Georgis, Jian Weng, Jessi Rodriguez, Hannah Rivett, Shadan Alrawi, Peng Li, and Wenjing Wang**

Abstract: Dopamine is a neurotransmitter essential for motor control, reward processing, and motivation through G-protein coupled receptor (GPCR) signaling. Recent GPCR-based real-time sensors allow for optical monitoring of dopamine release in behaving animals. However, there is still a need for high resolution mapping of dopamine release across large mouse brain volume for systemic studies. To fill this need, we have developed a new chimeric GPCR-based sensor to detect dopamine with a permanent green fluorescent mark through a combination of computational modeling and rational design. This new sensor, named "Single-chain Protein-based Ligand Indication through a Chimerically-Engineered Integrator Tool" (SPLICEIT), detects dopamine at cellular-resolution with high specificity and a fourfold signal-to-background ratio. We also developed a version of SPLICEIT whose signal can be normalized for varying sensor expression in cell culture and in vivo. This paves the way for further studies into dopamine release across the brain and enables the possibility of whole-brain dopamine mapping.

Introduction

Dopamine is an essential neuromodulator that is critical for roles from motor control to reward processing and motivation.[1–3] Dysfunctional dopamine signaling has been linked to addiction and neurological disorders such as schizophrenia and Parkinson's disease.[4–7] Dopaminergic neurons project throughout the brain and, upon their individual activation during specific behaviors, release dopamine to specific brain regions.[8] The effects of dopamine signaling are further dependent on the expression level and the distribution of the different classes of dopamine receptors in a given brain area, leading to combinatorial effects in cellular response.[9] Therefore, a full understanding of dopamine signaling, and its effects on various neuronal circuits, requires the development of a brain-map of dopamine release at high spatiotemporal resolution.

Numerous GPCR-based real-time fluorescent sensors have been developed to study neuromodulator transmission, including dopamine. Among these are the "GRAB"[10,11] and "Light"[12,13] sensor designs, which use the conformational change of the third intracellular loop of GPCRs (ICL3) to modulate the fluorescence of a circularly permuted fluorescent protein (cpFP).[10–15] The conformational shifts of the receptors change the local environment around the solvent-exposed fluorophore of the cpFP, modulating its brightness in a fast (within seconds) and reversible manner. The range in ligand affinity and specificity found in GPCRs allows development of tools for tracking specific neuromodulator releases with high spatiotemporal resolution.[12,14,16–25]

In addition to real-time sensors, "integrator" sensors have also been designed for detecting dopamine and other neuromodulators, leaving a long-lasting signal that persists after the experimental time-window. Most integrator sensors rely on multicomponent systems to release a transcription factor upon activation, which generates a long-lasting signal.[26–33] Other multicomponent integrator sensing methods are also being developed that do not rely on transcription factors, such as the faster reconstitution of split enzymes[34] or split fluorescent proteins.[35] These integrator sensors can allow for imaging of large areas of the brain, and even cell sorting for potential genetic profiling of activated cells.[28,30,32]

Our lab has previously designed an integrator sensor called "Single-chain protein-based opioid transmission

[*] S. M. Havens, B. Georgis, Dr. J. Weng, J. Rodriguez, H. Rivett, S. Alrawi, Prof. Dr. P. Li, Prof. Dr. W. Wang
Life Sciences Institute, University of Michigan, 210 Washtenaw Ave, Ann Arbor, MI 48109, USA
E-mail: wenjwang@umich.edu

S. M. Havens, B. Georgis, Dr. J. Weng, H. Rivett, Prof. Dr. W. Wang
Department of Chemistry, University of Michigan, 930 N University Ave, Ann Arbor, MI 48109, USA

Dr. J. Weng, J. Rodriguez, S. Alrawi, Prof. Dr. P. Li
Department of Biologic and Materials Sciences & Prosthodontics, University of Michigan, 1011 North University Ave, Ann Arbor, MI 48109, USA

Dr. J. Weng, J. Rodriguez, S. Alrawi, Prof. Dr. P. Li
Department of Molecular and Integrative Physiology, University of Michigan, 1301 Catherine St, Ann Arbor, MI 48109, USA

Additional supporting information can be found online in the Supporting Information section

© 2025 The Author(s). Angewandte Chemie International Edition published by Wiley-VCH GmbH. This is an open access article under the terms of the Creative Commons Attribution-NonCommercial-NoDerivs License, which permits use and distribution in any medium, provided the original work is properly cited, the use is non-commercial and no modifications or adaptations are made.

 © 2025 The Author(s). Angewandte Chemie International Edition published by Wiley-VCH GmbH

indicator tool" (SPOTIT).[36,37] SPOTIT has the advantage of using a single protein-chain design that avoids the difficulties inherent to balancing the expression of multiple components. SPOTIT generates a permanent fluorescent signal upon receptor activation by liberating cpGFP from Nb39—a nanobody initially designed to bind activated opioid receptors[38] that was also found to inhibit cpGFP fluorophore maturation.[36,37,39] However, the SPOTIT design only functions for opioid receptors due to the high specificity of Nb39 for opioid receptors over other GPCRs. "SPOTIT for all GPCRs" (SPOTall) successfully expanded the SPOTIT design for additional neuromodulators, including dopamine, through the addition of a second nanobody to regain conformation-specific affinity for alternative GPCR targets.[40] However, SPOTall exhibits much dimmer fluorescence than SPOTIT, and its application for other GPCRs requires the design of conformationally-specific nanobodies.

Here, we describe a new design to expand SPOTIT-based integrator sensors to additional neuromodulators. This new generalizable design is called "Single-chain Protein-based Ligand Indication through a Chimerically Engineered Integrator Tool", or SPLICEIT, which we demonstrate for detecting dopamine. Notably, dopamine-detecting SPLICEIT is brighter than our previous DRD1-SPOTall design, attaining a similar response to that seen in the brightness-improved M-SPOTIT2.[37] DRD3-SPLICEIT is small enough for packaging in adeno-associated virus (AAV) capsids with a second fluorescent protein expression marker to allow normalization between different expression levels, exhibiting a normalized signal-to-background ratio of fourfold. We demonstrate DRD3-SPLICEIT works in HEK293T cells, primary neuron cultures, mouse brain, and has a design generalizable to additional receptors.

Results and Discussion

Initial Design and Characterization of SPLICEIT for Detecting Dopamine

The SPOTall design successfully expanded the cpGFP-Nb39 sensor motif to nonopioid GPCRs through the addition of a second nanobody to act as the conformation-specific binding partner. However, multiple SPOTall designs exhibit much lower brightness than the original SPOTIT designs,[40] which affects its applications in animal experiments due to the high green autofluorescence seen in brain tissues.

We hypothesized that the disruption of the cpGFP-Nb39 interaction by the second nanobody in SPOTall may not be as efficient in removing Nb39 from cpGFP as full recruitment of Nb39 itself to the activated receptor, as in SPOTIT. Further, the stabilization of activated SPOTIT sensors was seen to increase the overall sensor protein level across cells, as well as the mean intensities[39] Controlling for this variability in protein level is also explored further, in later sections of this manuscript.

As chimeric receptors have a long history in the field of optogenetics,[41,42] we first envisioned a new design (Figure 1a) where the intracellular loops of the GPCR of interest were replaced with the intracellular loops of MOR. Consequently, the chimeric GPCR obtains the ability to directly bind with Nb39 upon receptor activation, removing Nb39 from cpGFP like that in SPOTIT.

We chose to start designing SPLICEIT for detecting dopamine due to its importance as a neuromodulator. There are five human dopamine GPCRs, split into two groups: "D_1-like" (D_1 and D_5), and "D_2-like" (D_2, D_3, and D_4).[8] GPCRs classically form a structure containing seven-transmembrane helixes, connected by three extracellular and three intracellular loop regions, with an extracellular ligand binding pocket and an intracellular region capable of initiating downstream intracellular signaling.[43–48] D_1-like receptors are $G\alpha_s$-coupled, leading to an increase in intracellular cAMP. D_2-like receptors are $G\alpha_i$-coupled, and instead lead to a decrease in intracellular cAMP.

To maximize our engineering success rate, we tested all five dopamine receptors for our SPLICEIT design. We utilized the online DeepTMHMM tool[49] to predict the membrane transition point for each of the seven transmembrane helices on each dopamine receptor and MOR. Additionally, the KOR C-terminal sequence, utilized in M-SPOTIT1.1 and M-SPOTIT2,[36,37] was used to link the chimeric receptor structure to the cpGFP-Nb39 motif. Through a combination of sequence alignment and structural alignment of the MOR crystal structure to dopamine receptor structures predicted by AlphaFold2,[50,51] sequence areas were selected for each transmembrane section where two sequential amino acids between each structure shared identity to limit perturbation of the helices. In this way, each chimeric receptor was constructed into the SPLICEIT design and tested in HEK cells for its response to 100 μM dopamine over a 24-h period (Figure 1b,c).

Three of the starting chimeric designs showed a significant response to incubation with dopamine: cD_3, cD_4, and cD_5 (Figure 1b), with the D_3 dopamine receptor chimeric version, cD_3, showing the largest dopamine-induced fluorescence increase and sensor brightness (Figure 1c). Notably, the cD_3 design showed a brightness increase similar to that of the improved M-SPOTIT2 sensor (Figure 2a). We therefore chose to further engineer and characterize this version of SPLICEIT based on cD_3, which is called DRD3-SPLICEIT1.0 from here on. DRD3-SPLICEIT1.0 displayed an EC_{50} of 8.4 μM to dopamine. This is much higher than the low nanomolar values previously observed for the native D_3 receptor (Figure 2b),[8,52,53] but closer to that of the "dLight" sensors based on the D_1 receptor.[54]

Further Optimization and Characterization of DRD3-SPLICEIT

As dopamine does not cross the cell membrane, trafficking of dopamine sensors to the plasma membrane is critical for detecting the released dopamine on the extracellular side. However, live cell anti-FLAG immunostaining, which would stain FLAG signal on the plasma membrane surface, showed DRD3-SPLICEIT1.0 had poor membrane trafficking. Close examination of DRD3-SPLICEIT1.0 revealed that the C-terminus of the initial cD3 construct contains an unintended

© 2025 The Author(s). Angewandte Chemie International Edition published by Wiley-VCH GmbH

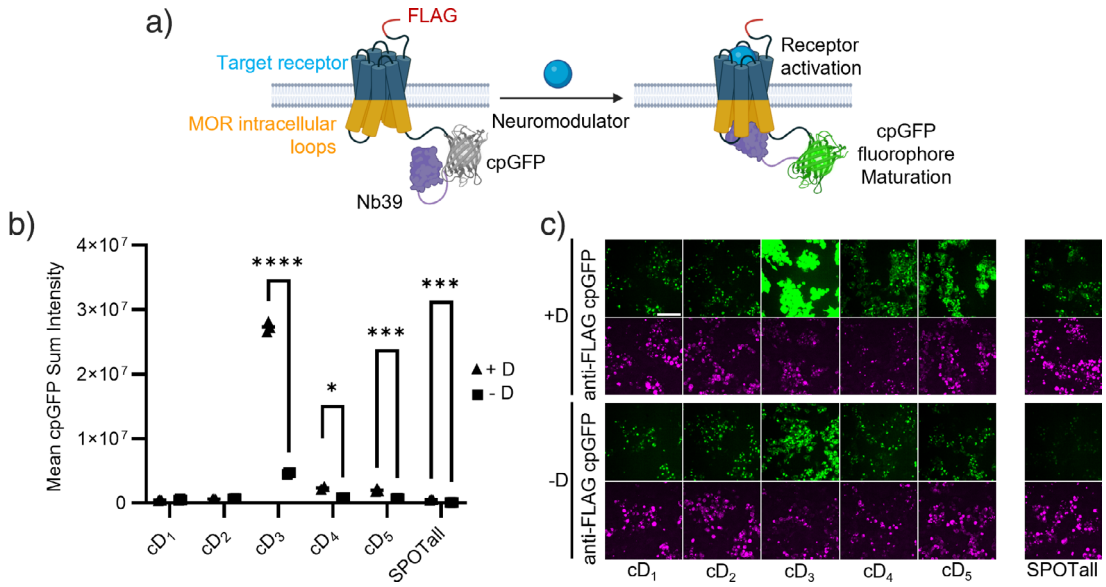


Figure 1. Characterization of initial dopamine receptor SPLICEIT designs. a) Diagram showing the SPLICEIT design. The intracellular regions of MOR are combined with the intermembrane and extracellular structure of the target receptor, allowing removal of Nb39 from cpGFP upon chimeric receptor activation by the target receptor agonist. b) Testing of initial dopamine receptor SPLICEIT designs. One day after SPLICEIT transfection, cells were stimulated with either 100 µM dopamine or equivalent volume of fresh growth media for 24 h and then fixed and immunostained for imaging at pH 11. $n = 3$ technical replicates, and the sum cpGFP fluorescence intensity was calculated for ten images per replicate. Each point represents the mean of the three technical replicates, errors bars representing the standard error of the mean. Stars indicate significance after performing an unpaired Student's t test: ****, p value < 0.0001, ***, p value < 0.001, and *, p value < 0.05. cD_1, cD_2, cD_3, cD_4, and cD_5, chimeric receptor design of dopamine receptor D_1, D_2, D_3, D_4, and D_5 with MOR; SPOTall, previously published dopamine sensor[40]; +D, 100 µM dopamine incubation; −D, fresh growth media incubation. c) Representative 20× confocal fluorescence images of data shown in (b), scale bar 100 µm. Immunostaining images displayed with 75 pixel radius rollingball background subtraction, for visual clarity only. cpGFP, cpGFP fluorescence; anti-FLAG, immunostaining fluorescence.

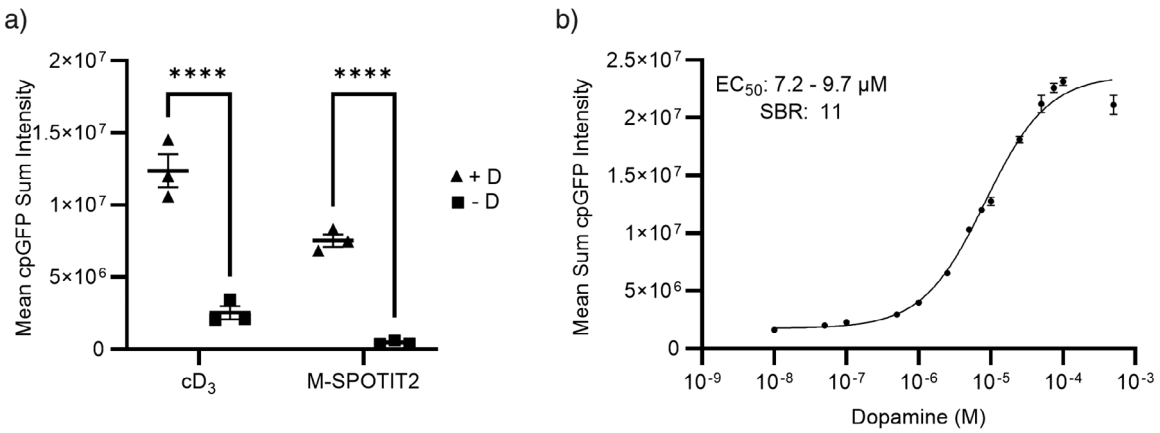


Figure 2. Characterization of DRD3-SPLICEIT1.0. a) Initial characterization of DRD3-SPLICEIT1.0 brightness, in comparison to M-SPOTIT2. Cells were stimulated and imaged as in Figure 1. +D, 100 µM dopamine for DRD3-SPLICEIT1.0 or 10 µM fentanyl for M-SPOTIT2; −D, equivalent volume of fresh cell growth media used in place of drug stimulation. Stars indicate significance after performing an unpaired Student's t test: ****, p value < 0.0001. b) Dopamine titration of cD_3. Cells were stimulated and imaged as in Figure 1, with varying amounts of dopamine. Each point represents the mean of three technical replicates with ten images each, error bars representing the standard error of the mean (some error bars not visualizable on graph). EC_{50} given as a 95% confidence interval. SBR, signal-to-background ratio, calculated by the ratio of the mean sum cpGFP intensity at the highest dopamine concentration to fresh cell growth media alone.

truncation at the palmitoylation site[55] of the D_3 receptor. Consequently, a potential key cysteine residue and four amino acids were inadvertently removed and prevented the palmitoylation and membrane anchoring of the C-terminus of the receptor, which likely led to the poor membrane trafficking.

Indeed, full restoration of these amino acids led to much improved trafficking, but also led to high background fluorescence in the absence of dopamine (data not shown). We, therefore, tested adding back the missing amino acids one at a time with the missing cysteine, as shown in (Figure 3a,b).

© 2025 The Author(s). Angewandte Chemie International Edition published by Wiley-VCH GmbH

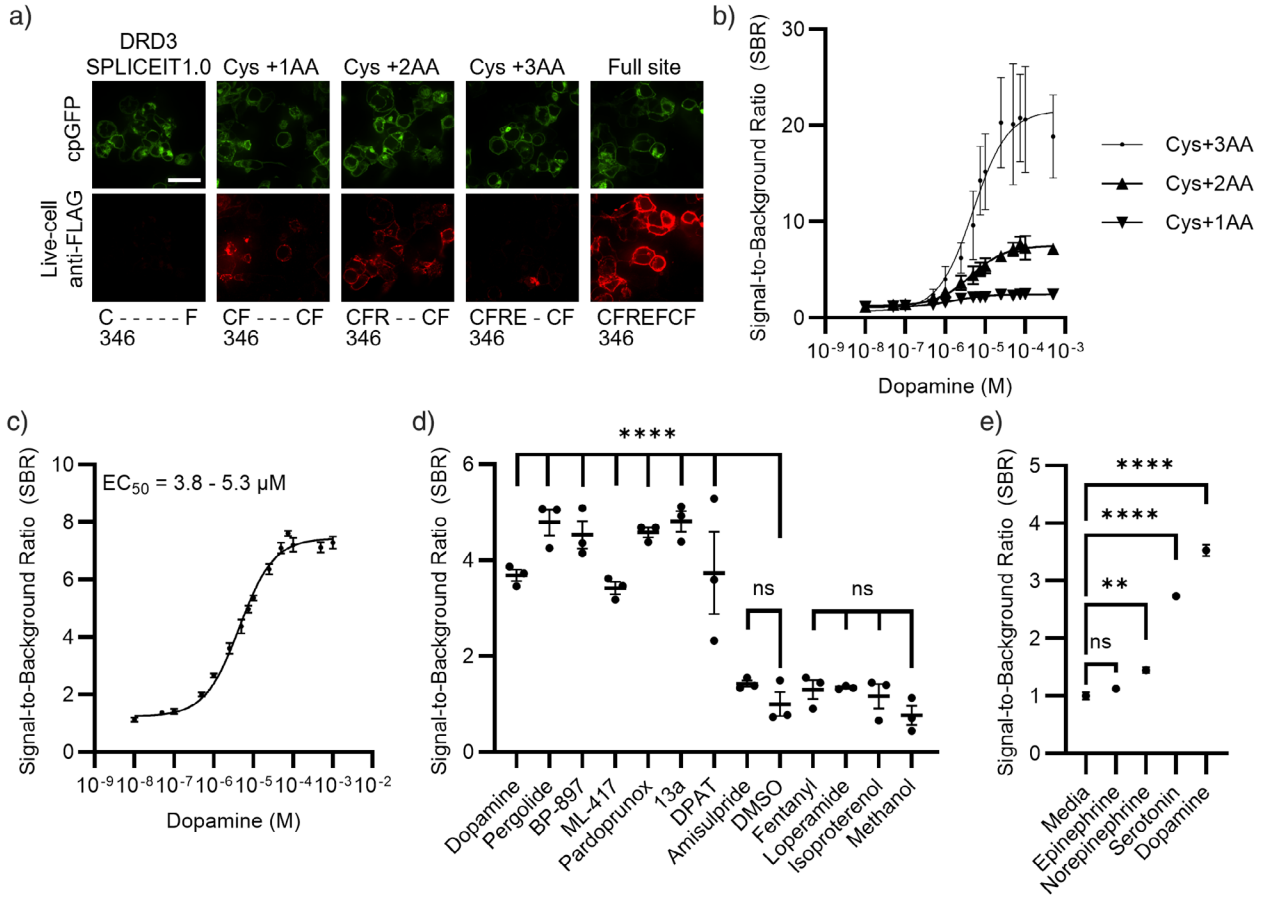


Figure 3. Design and characterization of DRD3-SPLICEIT1.1. a) Representative images comparing the membrane trafficking of SPLICEIT with varying palmitoylation-site lengths. One day after transfection, cells were stimulated with 100 µM dopamine for 24 h. Then, the cells were immunostained against the extracellular FLAG tag without cell membrane permeabilization, to visualize the degree of proper membrane trafficking. cpGFP, cpGFP fluorescence; anti-FLAG, membrane-trafficked protein expression. Scale bar 100 µm. Amino acid sequence given as bottom label"–" indicated missing residues. The cysteine residue number is given as 346(PDB:5C1M).[38] b) Analysis of dopamine titration for SPLICEIT with different palmitoylation site-lengths. Cells were stimulated as in (a), with varying amounts of dopamine as shown, before fixation and imaged at pH 11. $n = 3$ technical replicates. Signal-to-background ratio, the ratio of the mean of the sum fluorescence intensity measured with dopamine to that measured without dopamine. Each point represents the mean of each replicate; error bars, standard error of the mean. Lines indicate the best fit three parameter curve for each sensor. c) Revisualization of the dopamine titration of Cys + 2AA, now referred to as DRD3-SPLICEIT1.1, as shown and analyzed in (a). d) Analysis of DRD3-SPLICEIT1.1′s response to various dopamine and opioid receptor ligands, with control conditions containing the equivalent amount of DMSO or methanol from each drug addition. Cells were stimulated with 10 µM of each drug shown, imaging and analysis as in (a). e) Analysis of DRD3-SPLICEIT1.1′s response to nondopamine endogenous ligands with potential for activating native dopamine receptors. Cells were stimulated, imaged, and analyzed as in (d). Stars indicate significance after performing a one-way ANOVA, with comparison of the mean of each condition to either DMSO, methanol, or growth media control conditions as displayed; ** p value < 0.01; **** p value < 0.0001. EC_{50} given as a 95% confidence interval.

We characterized both the dopamine response as well as the membrane trafficking (Figure 3a). Of the three constructs tested, the reincorporation of the missing cysteine and two amino acids demonstrated the best balance of membrane trafficking and signal-to-background ratio (SBR) (Figure 3b) and was therefore chosen to be DRD3-SPLICEIT1.1. This new DRD3-SPLICEIT1.1 design also exhibited a slightly improved EC_{50} (Figure 3c), likely due to the improved membrane trafficking. As dopamine has been shown to favor a membrane-dependent mechanism for receptor activation,[56] increased membrane trafficking is likely to increase the sensor population activated and stabilized by dopamine binding.

DRD3-SPLICEIT1.1 also demonstrated selectivity for known dopamine receptor agonists, with no significant response to other common GPCR ligands (Figure 3d). Notably, DRD3-SPLICEIT1.1 showed a strong response to multiple synthetic agonists with selectivity for the D_3 dopamine receptor: BP-897,[57] ML-417,[58] and the cariprazine analogue 13a.[59] This indicates that the binding pocket of the chimeric design likely retains a similar structure to that of the native receptor while intracellularly retaining the ability to recruit Nb39 upon activation.

Further, DRD3-SPLICEIT1.1 was also tested for response against neuromodulators known to activate D_2-like receptors in the brain (Figure 3e).[60–62] This sensor showed a strong response to serotonin, a moderate response to norepinephrine, and no statistically relevant response to epinephrine.

© 2025 The Author(s). Angewandte Chemie International Edition published by Wiley-VCH GmbH

Designing and Characterization of Ratiometric DRD3-SPLICEIT2.0 in Cell Cultures

DRD3-SPLICEIT1.1 is smaller than that of the SPOTall design, opening room for additional components to be added while retaining high packaging efficiency for AAV production. One challenge of integrator sensors can be compensating for varying expression levels between conditions. Designing a ratiometric integration sensor, in which the sensor signal can be normalized to the expression level, will significantly improve the consistency of sensor performance. For SPOTIT and SPOTIT-like sensors, immunostaining of the sensor with and without agonists could not be used for protein expression normalization. This is because the sensor is stabilized by receptor activation, leading to a higher final expression level in the presence of agonists, which acts as part of the sensor activation mechanism.[39,40] Therefore, we intend to introduce a second fluorescent protein to indicate the overall protein expression amount separate from the stability of the sensor itself.

To prevent the protein expression level readout from being affected by the sensor, a C-terminal P2A peptide sequence was used. The P2A sequence is derived from the porcine teschovirus-1 and "self-cleaves" a peptide chain during translation through a ribosomal skipping mechanism.[63] This mechanism is ideal for normalizing the expression of a SPOTIT-like sensor as it allows expression of the secondary FP from the same mRNA strand as the sensor without being affected by the protein-structure instability of the inactive sensor. This design was deemed DRD3-SPLICEIT2.0.

Incorporation of the second FP via P2A successfully allowed multichannel imaging of the sensor (Figure 4), which will provide a more consistent SBR across experiments when used for ratiometric analysis. Indeed, mCherry's protein level was not affected by dopamine (Figure 4a). Comparison of the mCherry's increased expression over time to the sensor's leveled off signal in the absence of dopamine (Figure 4b) provides further evidence that SPOTIT-type sensors are unstable and degrade over time in the absence of agonists. In contrast, the cpGFP fluorescence of the sensor increases over time in the presence of dopamine as a result of the cpGFP fluorophore maturation upon removal of Nb39 and stabilization of the sensor. Comparison of final fluorescence intensities alongside immunostaining (Figure 4c,d) confirms that the p2a-expressed mCherry marker is not affected by the changing stability of the sensor and can therefore be used to more accurately account for variation in protein expression levels.

With the successful application of an expression marker into the system, this tool design was further characterized for titration response to dopamine and synthetic agonists shown to activate DRD3-SPLICEIT1.1. DRD3-SPLICEIT2.0 shows a similar EC_{50} response to dopamine as DRD3-SPLICEIT1.1, as expected (Figure 4e). DRD3-SPLICEIT2.0 also showed response to high concentrations of norepinephrine with an EC_{50} of 53 μM, which is not surprising as norepinephrine is a catecholamine known to interact with dopamine receptors.[61] DRD3-SPLICEIT2.0 also exhibits an EC_{50} of 8.6 μM for serotonin, which is consistent with the micromolar-range binding affinity seen in other dopamine receptors,[64,65] allowing potential detection of serotonin as well. DRD3-SPLICEIT2.0 also shows strong response to the synthetic agonists BP-897[57] and the cariprazine analogue 13a[59] in the nanomolar range, demonstrating its capability for integrating signals from low concentrations of agonists.

An additional benefit of integration sensors is the option for postexperimental analysis of positive cells. As a proof of concept that the SLICEIT design allows for the separation of such activated cells postexperiment, DRD3-SPLICEIT2.0 was analyzed through fluorescence activated cell sorting (FACS). HEK cells for FACS analysis were transfected with DRD3-SPLICEIT2.0 for one day, before incubation for an additional day with fresh cell growth media either alone or containing 100 μM dopamine. Utilizing the p2a mCherry as an expression marker and cpGFP fluorescence as the activation signal, the two cell populations were then analyzed through FACS (Figure 4f) and a clear increase in activation signal was seen for the cells incubated with dopamine.

This allowed generation of simple quadrants separating positive cpGFP and mCherry signals, where Q2 contains only 0.55% of the cells untreated with dopamine versus 5.27% of cells treated with dopamine. Using FACS in this way would allow comparison of activated versus nonactivated cells for transcriptomic or other postexperimental techniques to further our understanding of the characteristics of activated cells in areas surrounding neuromodulator release.

Characterization of DRD3-SPLICEIT2.0 in Primary Neuronal Cultures and Mouse Brain

As the eventual goal is to map dopamine release throughout the brain, we next packaged DRD3-SPLICEIT2.0 in AAV for characterization in primary neuronal cultures. We used a ubiquitous promoter, cytomegalovirus early enhancer/chicken β-actin promoter (CAG), to drive the expression of DRD3-SPLICEIT2.0, so that it can be expressed in both neurons and glial cells, maximizing the detection of dopamine across the brain. The cultured neurons were infected with AAV encoding DRD3-SPLICEIT2.0. Six days postinfection, the neuronal culture was stimulated with dopamine and incubated for 24 h. Bright green fluorescence was observed in the dopamine-stimulated condition, whereas mCherry expression was high in both with and without dopamine conditions (Figure 5a). A ratiometric SBR of 4 was observed (Figure 5b), performing similarly to that seen in HEK cells.

With successful ratiometric response in neurons, we moved on to demonstrate the potential application of SPLICEIT in mouse brains. All experimental procedures were carried out in accordance with the animal care standards in NIH guidelines and approved by the University Committee on Use and Care of Animals at the University of Michigan. AAV encoding DRD3-SPLICEIT2.0 was injected into the lateral hypothalamic area (LHA) and allowed six days to express before intracerebroventricular injection of either dopamine or saline. One day after drug administration, each mouse was deeply anesthetized before brain removal and imaging. As can be seen in Figure 5c, there was notable increase in tool expression (as seen through mCherry

© 2025 The Author(s). Angewandte Chemie International Edition published by Wiley-VCH GmbH

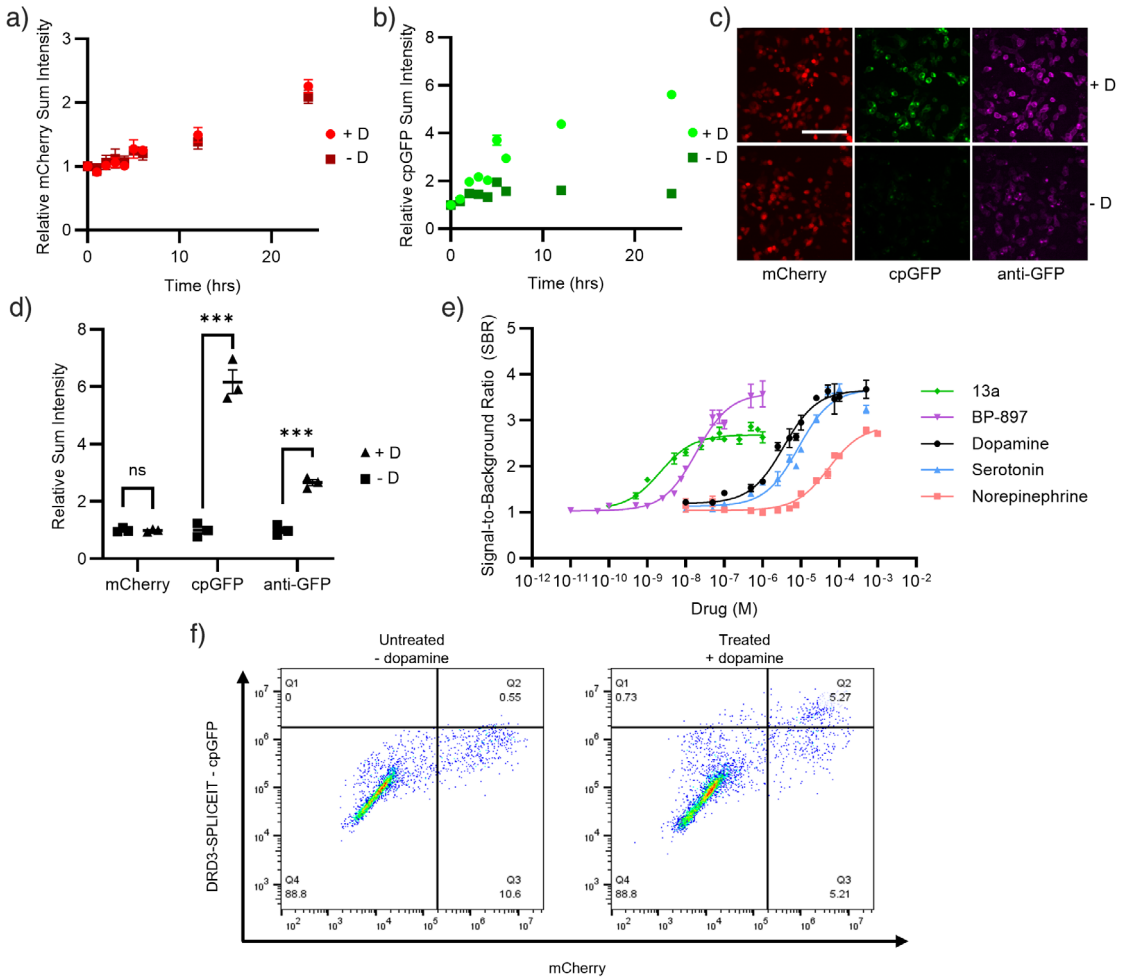


Figure 4. Design and characterization of DRD3-SPLICEIT2.0. a) Analysis of mCherry fluorescence development over time, with and without the presence of dopamine. One day after transfection, cells were incubated for 24 h with either 100 μM dopamine (+D) or fresh media (−D) as a control. Cells were imaged live in growth media at indicated time points. Sum Intensity at each time point was then normalized to the starting 0 h sum intensity. b) Analysis of sensor's cpGFP fluorescence development from cells in (a). c) Representative images of cells transfected and stimulated as in (a) and (b), with fixation after 24 h of incubation for imaging at pH 11. mCherry, mCherry expression marker fluorescence; cpGFP, cpGFP fluorescence; antiGFP, immunostaining fluorescence. Scale bar 100 μm. Immunostaining images displayed with 75 pixel radius rollingball background subtraction, for visual clarity only. d) Analysis of cells shown in (c), with each fluorescent signal analyzed as in Figure 2 before normalization to the fluorescent signal present in the −D condition to generate relative sum intensities. Stars indicate significance after performing an unpaired Student's *t* test, with three stars indicating a *p* value < 0.001. e) Analysis of DRD3-SPLICEIT2.0 dose response to titration with synthetic dopamine receptor agonists 13a (EC_{50}: 1.6–4.6 nM) and BP-897 (EC_{50}: 15–25 nM), dopamine (EC_{50}: 2.5–4.9 μM), serotonin (EC_{50}: 6.3–12 μM), and norepinephrine (EC_{50}: 40–69 μM). Cells were stimulated and imaged as in Figure 3c, with ratiometric sensor response instead calculated by dividing the calculated cpGFP sum intensities of each image by their respective mCherry sum intensity. Signal-to-background ratio calculated by dividing the ratiometric response at the highest concentration of agonist by response with fresh growth media alone. f) Fluorescence activated cell sorting can identify activated DRD3-SPLICEIT2.0. The mCherry fluorescence serves as an expression marker and the cpGFP fluorescence as the sensor activation signal. Each population was analyzed for 10 000 events. Dopamine treated cells saw ~10-fold enrichment in the Q2 quadrant in comparison to untreated cells. Q1, high sensor activation and low expression; Q2, high sensor activation and high expression, Q3, low sensor activation with high expression; and Q4, low sensor activation and low expression.

fluorescence) in the presence of dopamine—reinforcing the importance of controlling for sensor expression between conditions. There was a twofold increase in ratiometric response to dopamine in comparison to saline controls, as seen in Figure 5d, demonstrating the potential of DRD3-SPLICEIT2.0 to be applied in vivo to detect dopamine release across large brain volumes. However, further optimization will be required to increase the activation efficiency in mouse brains.

Extending the SPLICEIT Design to Detect Other Neuromodulators

Finally, the generalizability of the SPLICEIT design was investigated. A computational screening method would aid in the development of new designs, and so we first investigated the predicted binding energy of each of the initial dopamine sensor designs. The AlphaFold2-generated structure of each initial chimeric dopamine receptor design, ending at the

© 2025 The Author(s). Angewandte Chemie International Edition published by Wiley-VCH GmbH

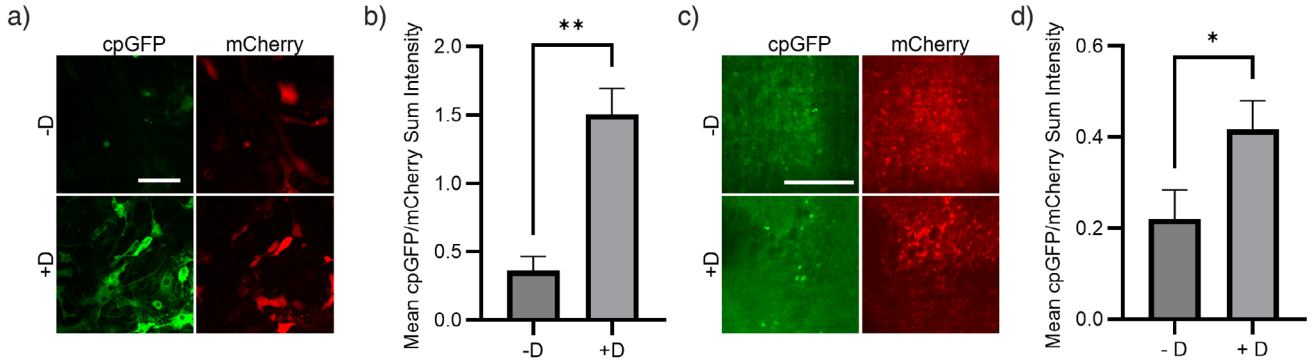


Figure 5. Response of DRD3-SPLICEIT2.0 in neuron culture and mouse brains. a) Representative images showing cpGFP signal response and mCherry expression marker in rat whole brain cultured neurons. Six days after infection with AAV-virus containing SPLICEIT, neurons were stimulated with 100 µM dopamine (+D) or fresh growth medium(−D) for 24 h in triplicate. Cells were fixed and imaged at pH 11. Scale bar 100 µm. cpGFP, cpGFP fluorescence; mCherry, p2a expression marker fluorescence. b) Analysis of data from (a), with each dot showing the mean ratio of cpGFP/mCherry sum intensity for 10 fields of view per replicate. c) Representative cpGFP images of DRD3-SPLICEIT2.0 response in mouse brain, after cyrosectioning through the LHA region. Images cropped to regions of highest expression, for display only. On Day 0, AAV encoding DRD3-SPLICEIT2.0 was injected into LHA. On Day 6, 1 µmol kg^{-1} dopamine (+D) or saline (−D) was administered through intracerebroventricular injection. Scale bar 250 µm. d) Statistics of experiment described in (c). The mean cpGFP/mCherry sum intensity of the five highest-expressing brain slices per mouse are plotted for each condition, with three mice each. Error bars indicate SEM. Stars indicate significance after performing an unpaired Student's *t* test; *, *p* value < 0.05; **, *p* value < 0.01.

palmitoylation site, was used to estimate the predicted binding energy with Nb39 through Rosetta with RosettaDock[66] and InterfaceAnalyzer[67] (Figure 6a). The chimeric DRD3 version showed the most similar binding energy to that of the native MOR structure, supporting the hypothesis that this computational method may be beneficial for prescreening receptor designs.

Next, chimeric designs for 11 additional GPCRs were examined for predicted binding affinity to Nb39 (Figure 6b). The screened designs included several adrenergic and serotonergic receptors, as well as the cannabinoid receptor 2 and the muscarinic acetylcholine receptor M2. The five receptor designs with the best binding energy were selected for testing using the SPLICEIT design and new potential sensors for norepinephrine, cα_2AR, and serotonin, c5-HT_{1B}, were found (Figure 6c,d). The remaining two chimeric serotonin receptors also showed promise with much higher SBR responses; however they also demonstrated much lower sensitivity than c5-HT_{1B} (Figure S1). The cCB2 receptor was the only receptor in the top five to not show a dose response (Figure S1). This demonstrates the generalizability of the chimeric receptor design and a great potential for further development of additional GPCR-based integrator sensors that could be tuned and improved through directed evolution for greater sensitivity and/or selectivity.

Conclusion

Here, we have shown a new single-chain fluorescence integration sensor design called SPLICEIT. By designing chimeric GPCRs that are bifunctional, the ligand selectivity of the GPCR facing the extracellular side and the ability to recruit Nb39 upon receptor activation are both retained. We demonstrated its application by designing DRD3-SPLICEIT2.0 for detecting dopamine, where it shows a much brighter fluorescent signal than the existing DRD1-SPOTall. DRD3-SPLICEIT2.0 also introduced an additional fluorescent protein via P2A peptide for normalizing the sensor expression level, which will provide a more consistent expression-normalized SBR of around fourfold.

DRD3-SPLICEIT2.0 will have multiple applications in vitro and in vivo. It can detect dopamine with an EC_{50} of 3.5 µM and other potent dopamine receptor agonists in the range of low nanomolar values. Therefore, DRD3-SPLICEIT2.0 can potentially be used for characterizing and screening dopamine receptor agonists. Interestingly, DRD3-SPLICEIT2.0 can detect norepinephrine with low sensitivity and can detect serotonin in the similar micromolar value range as dopamine. This opens up new potential applications for detecting serotonin, although this limitation in specificity should be taken into account for experiments where notable dopamine and serotonin concentrations are both expected. We also demonstrated the feasibility of this sensor for use in cultured neurons and mouse brains to interrogate neuromodulator signaling in the brain. DRD3-SPLICEIT2.0 offers potential for a preliminary broad screen in cell cultures or in animal models across the brain, which can be followed up with other sensors for further investigation.

The SPLICEIT design is also generalizable for the development of GPCR-based integrator sensors. We developed a computational modeling-based screening method for the expansion of this design to additional receptors and demonstrated its feasibility with two additional SPLICEIT designs for detecting norepinephrine and serotonin.

Although SPLICEIT demonstrates potential applications, it also has limitations. The SBRs of the DRD3-SPLICEIT2.0 can potentially be further improved by developing Nb39 variants that show reduced binding to the inactive receptor.

© 2025 The Author(s). Angewandte Chemie International Edition published by Wiley-VCH GmbH

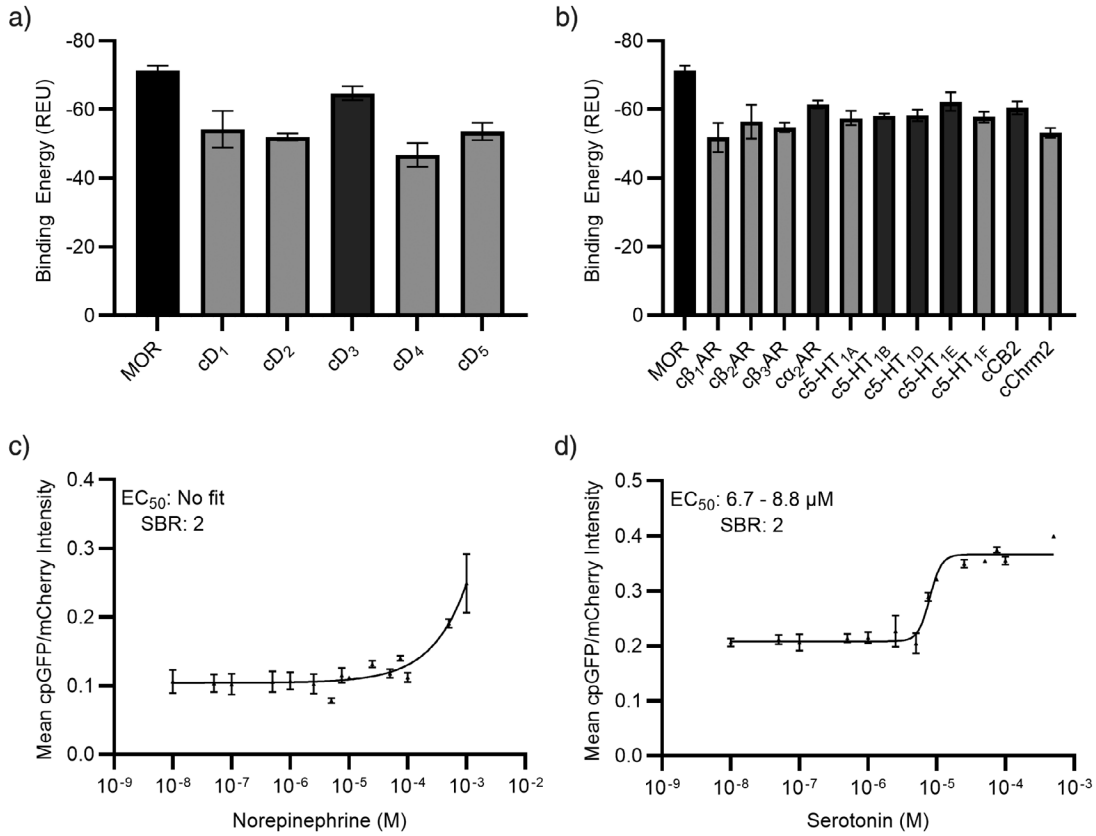


Figure 6. Generalizability of the SPLICEIT design. a) Comparison of calculated binding energies between MOR or chimeric dopamine receptors against Nb39. Each receptor structure was modeled up to the palmitoylation site using AlphaFold2 and aligned with the MOR/NB39 crystal structure (PDB: 5C1M)[1]. The resulting modeled MOR/Nb39 or chimeric receptor/Nb39 pairs were then redocked through RosettaDock for 1000 potential structures, and the top 10% of total scoring designs analyzed with Rosetta InterfaceAnalyzer. The binding energy of the top 10 designs for each pair is then plotted and shown. b) Additional potential chimeric receptor designs, analyzed as in (a). Darkened columns signify receptor designs chosen for further investigation. c) Norepinephrine titration of α_2AR-SPLICEIT1.0 in HEK293T/17 cells. One day after transfection, cells were incubated in triplicate with noted concentrations of norepinephrine or fresh media for 24 h. Cells were then fixed and imaged at pH 11, with the mean cpGFP/mCherry sum intensity calculated for 10 images per replicate. Each point indicates the mean of three replicates. Error bars, standard error of the mean. EC_{50}, best fit value analysis with three parameters given as 95% confidence interval; SBR, ratio of the mean ratiometric response at the highest concentration of ligand to the ratiometric response in the absence of ligand. d) Serotonin titration of 5-HT_{1B}-SPLICEIT1.0, cells treated and analyzed as in (c).

The sensitivity of DRD3-SPLICEIT2.0 can also be tuned higher or lower by modifying the DRD3 binding pocket to have an array of integration sensors for detecting dopamine in a wide range, as frequently seen in real-time sensor development. Even though SPLICEIT is generalizable, it is most suitable for Gα_i-coupled receptors and new designs need to be developed to generalize SPLICEIT for Gα_s- and Gα_q-coupled receptors.

Overall, SPLICEIT represents a new fluorescence integrator design and opens up many opportunities for engineering new fluorescence integration sensors for detecting a range of neuromodulators.

Supporting Information

The authors have cited additional references within the Supporting Information.[68]

Acknowledgements

W.W. was supported by the University of Michigan, the NIH (DP2MH132939, R01DA053200), the Camille Dreyfus and Henry Foundation (TC-23-084) and the Sloan Research Fellowships FG-2024-22156. P.L. was supported by University of Michigan, the NIH (R01AT011652 and R01HL156989).

Conflict of Interests

The authors declare no conflict of interest.

Data Availability Statement

The data that support the findings of this study are available from the corresponding author upon reasonable request.

© 2025 The Author(s). Angewandte Chemie International Edition published by Wiley-VCH GmbH

Keywords: Chimeric • CpGFP • Dopamine • Fluorescent sensor • GPCR

[1] R. A. Wise, *Philosoph. Trans. Royal Soc. B: Biol. Sci.* **2006**, *361*, 1149–1158.
[2] S. Ge, C. Yang, M. Li, J. Li, X. Chang, J. Fu, L. Chen, C. Chang, X. Wang, J. Zhu, G. Gao, *Brain Res.* **2012**, *1465*, 66–79.
[3] M. O. Klein, D. S. Battagello, A. R. Cardoso, D. N. Hauser, J. C. Bittencourt, R. G. Correa, *Cell. Mol. Neurobiol.* **2019**, *39*, 31–59.
[4] K. Szafran, A. Faron-Górecka, M. Kolasa, M. Kuśmider, J. Solich, D. Żurawek, M. Dziedzicka-Wasylewska, *Pharm. Rep.* **2013**, *65*, 1498–1505.
[5] Y. Huang, N. Todd, A. Thathiah, *Curr. Opin. Pharmacol.* **2017**, *32*, 96–110.
[6] M. Guerram, L.-Y. Zhang, Z.-Z. Jiang, *Neurochem. Int.* **2016**, *101*, 1–14.
[7] M. Solinas, P. Belujon, P. O. Fernagut, M. Jaber, N. Thiriet, *J. Neural Transmiss.* **2019**, *126*, 481–516.
[8] R. Pivonello, D. Ferone, G. Lombardi, A. Colao, S. Lamberts, L. Hofland, *Euro. J. Endocrin.* **2007**, *156*, S13–S21.
[9] C. Liu, P. Goel, P. S. Kaeser, *Nat. Rev. Neurosci.* **2021**, *22*, 345–358.
[10] Y. Zhuo, B. Luo, X. Yi, H. Dong, X. Miao, J. Wan, J. T. Williams, M. G. Campbell, R. Cai, T. Qian, F. Li, S. J. Weber, L. Wang, B. Li, Y. Wei, G. Li, H. Wang, Y. Zheng, Y. Zhao, M. E. Wolf, Y. Zhu, M. Watabe-Uchida, Y. Li, *Nat. Methods* **2024**, *21*, 680–691.
[11] F. Deng, J. Wan, G. Li, H. Dong, X. Xia, Y. Wang, X. Li, C. Zhuang, Y. Zheng, L. Liu, Y. Yan, J. Feng, Y. Zhao, H. Xie, Y. Li, *Nat. Methods* **2024**, *21*, 692–702.
[12] F. Sun, J. Zeng, M. Jing, J. Zhou, J. Feng, S. F. Owen, Y. Luo, F. Li, H. Wang, T. Yamaguchi, Z. Yong, Y. Gao, W. Peng, L. Wang, S. Zhang, J. Du, D. Lin, M. Xu, A. C. Kreitzer, G. Cui, Y. Li, *Cell* **2018**, *174*, 481–496.e419.
[13] T. Patriarchi, A. Mohebi, J. Sun, A. Marley, R. Liang, C. Dong, K. Puhger, G. O. Mizuno, C. M. Davis, B. Wiltgen, M. Von Zastrow, J. D. Berke, L. Tian, *Nat. Methods* **2020**, *17*, 1147–1155.
[14] T. Patriarchi, J. R. Cho, K. Merten, M. W. Howe, A. Marley, W. H. Xiong, R. W. Folk, G. J. Broussard, R. Q. Liang, M. J. Jang, H. N. Zhong, D. Dombeck, M. von Zastrow, A. Nimmerjahn, V. Gradinaru, J. T. Williams, L. Tian, *Science* **2018**, *360*.
[15] M. Jing, Y. Zhang, H. Wang, Y. Li, *J. Neurochem.* **2019**, *151*, 279–288.
[16] M. Jing, P. Zhang, G. Wang, J. Feng, L. Mesik, J. Zeng, H. Jiang, S. Wang, J. C. Looby, N. A. Guagliardo, *Nat. Biotechnol.* **2018**, *36*, 726–737.
[17] M. Jing, Y. Li, J. Zeng, P. Huang, M. Skirzewski, O. Kljakic, W. Peng, T. Qian, K. Tan, J. Zou, S. Trinh, R. Wu, S. Zhang, S. Pan, S. A. Hires, M. Xu, H. Li, L. M. Saksida, V. F. Prado, T. J. Bussey, M. A. M. Prado, L. Chen, H. Cheng, Y. Li, *Nat. Methods* **2020**, *17*, 1139–1146.
[18] J. Feng, C. Zhang, J. E. Lischinsky, M. Jing, J. Zhou, H. Wang, Y. Zhang, A. Dong, Z. Wu, H. Wu, W. Chen, P. Zhang, J. Zou, S. A. Hires, J. J. Zhu, G. Cui, D. Lin, J. Du, Y. Li, *Neuron* **2019**, *102*, 745–761.e748.
[19] C. Dong, C. Ly, L. E. Dunlap, M. V. Vargas, J. Sun, I.-W. Hwang, A. Azinfar, W. C. Oh, W. C. Wetsel, D. E. Olson, *Cell* **2021**, *184*, 2779–2792.e2718.
[20] C. Dong, R. Gowrishankar, Y. Jin, X. J. He, A. Gupta, H. Wang, N. Sayar-Atasoy, R. J. Flores, K. Mahe, N. Tjahjono, R. Liang, A. Marley, G. Or Mizuno, D. K. Lo, Q. Sun, J. L. Whistler, B. Li, I. Gomes, M. Von Zastrow, H. A. Tejeda, D. Atasoy, L. A. Devi, M. R. Bruchas, M. R. Banghart, L. Tian, *Nat. Neurosci.* **2024**, *27*, 1844–1857.
[21] Z. Wu, K. He, Y. Chen, H. Li, S. Pan, B. Li, T. Liu, F. Xi, F. Deng, H. Wang, J. Du, M. Jing, Y. Li, *Neuron* **2022**, *110*, 770–782.e775.
[22] A. Dong, K. He, B. Dudok, J. S. Farrell, W. Guan, D. J. Liput, H. L. Puhl, R. Cai, H. Wang, J. Duan, *Nat. Biotechnol.* **2022**, *40*, 787–798.
[23] W. Peng, Z. Wu, K. Song, S. Zhang, Y. Li, M. Xu, *Science* **2020**, *369*, eabb0556.
[24] H. Wang, T. Qian, Y. Zhao, Y. Zhuo, C. Wu, T. Osakada, P. Chen, Z. Chen, H. Ren, Y. Yan, L. Geng, S. Fu, L. Mei, G. Li, L. Wu, Y. Jiang, W. Qian, L. Zhang, W. Peng, M. Xu, J. Hu, M. Jiang, L. Chen, C. Tang, Y. Zhu, D. Lin, J.-N. Zhou, Y. Li, *Science* **2023**, *382*, 3.
[25] M. Kauk, C. Hoffmann, *Trends Pharmacol. Sci.* **2018**, *39*, 123–135.
[26] G. Barnea, W. Strapps, G. Herrada, Y. Berman, J. Ong, B. Kloss, R. Axel, K. J. Lee, *Proc. Natl. Acad. Sci. USA* **2008**, *105*, 64–69.
[27] W. K. Kroeze, M. F. Sassano, X.-P. Huang, K. Lansu, J. D. McCorvy, P. M. Giguère, N. Sciaky, B. L. Roth, *Nat. Struct. Mol. Biol.* **2015**, *22*, 362–369.
[28] D. Lee, M. Creed, K. Jung, T. Stefanelli, D. J. Wendler, W. C. Oh, N. L. Mignocchi, C. Lüscher, H.-B. Kwon, *Nat. Methods* **2017**, *14*, 495–503.
[29] M. Talay, E. B. Richman, N. J. Snell, G. G. Hartmann, J. D. Fisher, A. Sorkaç, J. F. Santoyo, C. Chou-Freed, N. Nair, M. Johnson, J. R. Szymanski, G. Barnea, *Neuron* **2017**, *96*, 783–795.e784.
[30] M. W. Kim, W. Wang, M. I. Sanchez, R. Coukos, M. von Zastrow, A. Y. Ting, *Elife* **2017**, *6*, e30233.
[31] C. K. Kim, K. F. Cho, M. W. Kim, A. Y. Ting, *Elife* **2019**, *8*, e43826.
[32] M. I. Sanchez, A. Y. Ting, *Nat. Methods* **2020**, *17*, 167–174.
[33] W. Wang, *ACS Chem. Biol.* **2024**, *19*, 788–797.
[34] G. Zhou, W. W. Wan, W. Wang, *J. Am. Chem. Soc.* **2022**, *144*, 22933–22940.
[35] Q. Zhang, Y. W. Zheng, S. R. Coughlin, X. Shu, *Protein Sci.* **2018**, *27*, 874–879.
[36] K. E. Kroning, W. Wang, *Angew. Chem. Int. Ed.* **2021**, *60*, 13358–13365.
[37] K. E. Kroning, M. Li, D. I. Petrescu, W. Wang, *Chem. Commun.* **2021**, *57*, 10560–10563.
[38] W. Huang, A. Manglik, A. J. Venkatakrishnan, T. Laeremans, E. N. Feinberg, A. L. Sanborn, H. E. Kato, K. E. Livingston, T. S. Thorsen, R. C. Kling, S. Granier, P. Gmeiner, S. M. Husbands, J. R. Traynor, W. I. Weis, J. Steyaert, R. O. Dror, B. K. Kobilka, *Nature* **2015**, *524*, 315–321.
[39] K. E. Kroning, M. Li, J. Shen, H. Fiel, M. Nassar, W. Wang, *ACS Chem. Biol.* **2022**, *17*, 2212–2220.
[40] K. Kroning, N. Gannot, X. Li, A. Putansu, G. Zhou, J. Sescil, J. Shen, A. Wilson, H. Fiel, P. Li, W. Wang, *Proc. Natl. Acad. Sci. USA* **2024**, *121*, e2307090121.
[41] K. Deisseroth, *Nat. Neurosci.* **2015**, *18*, 1213–1225.
[42] R. D. Airan, K. R. Thompson, L. E. Fenno, H. Bernstein, K. Deisseroth, *Nature* **2009**, *458*, 1025–1029.
[43] B. Sun, D. Feng, M. L. Chu, I. Fish, S. Lovera, Z. A. Sands, S. Kelm, A. Valade, M. Wood, T. Ceska, T. S. Kobilka, F. Lebon, B. K. Kobilka, *Nat. Commun.* **2021**, *12*, 3305.
[44] S. G. Rasmussen, B. T. DeVree, Y. Zou, A. C. Kruse, K. Y. Chung, T. S. Kobilka, F. S. Thian, P. S. Chae, E. Pardon, D. Calinski, J. M. Mathiesen, S. T. Shah, J. A. Lyons, M. Caffrey, S. H. Gellman, J. Steyaert, G. Skiniotis, W. I. Weis, R. K. Sunahara, B. K. Kobilka, *Nature* **2011**, *477*, 549–555.
[45] S. G. Rasmussen, H. J. Choi, J. J. Fung, E. Pardon, P. Casarosa, P. S. Chae, B. T. Devree, D. M. Rosenbaum, F. S. Thian, T. S. Kobilka, A. Schnapp, I. Konetzki, R. K. Sunahara, S. H. Gellman, A. Pautsch, J. Steyaert, W. I. Weis, B. K. Kobilka, *Nature* **2011**, *469*, 175–180.

© 2025 The Author(s). Angewandte Chemie International Edition published by Wiley-VCH GmbH

[46] R. Nygaard, Y. Zou, R. O. Dror, T. J. Mildorf, D. H. Arlow, A. Manglik, A. C. Pan, C. W. Liu, J. J. Fung, M. P. Bokoch, F. S. Thian, T. S. Kobilka, D. E. Shaw, L. Mueller, R. S. Prosser, B. K. Kobilka, *Cell* **2013**, *152*, 532–542.
[47] N. R. Latorraca, A. J. Venkatakrishnan, R. O. Dror, *Chem. Rev.* **2017**, *117*, 139–155.
[48] F. Wu, G. Song, C. De Graaf, R. C. Stevens, *J. Mol. Biol.* **2017**, *429*, 2726–2745.
[49] J. Hallgren, K. D. Tsirigos, M. D. Pedersen, J. J. Almagro Armenteros, P. Marcatili, H. Nielsen, A. Krogh, O. Winther, bioRxiv, **2022**.
[50] J. Jumper, R. Evans, A. Pritzel, T. Green, M. Figurnov, O. Ronneberger, K. Tunyasuvunakool, R. Bates, A. Žídek, A. Potapenko, A. Bridgland, C. Meyer, S. A. A. Kohl, A. J. Ballard, A. Cowie, B. Romera-Paredes, S. Nikolov, R. Jain, J. Adler, T. Back, S. Petersen, D. Reiman, E. Clancy, M. Zielinski, M. Steinegger, M. Pacholska, T. Berghammer, S. Bodenstein, D. Silver, O. Vinyals, A. W. Senior, K. Kavukcuoglu, P. Kohli, D. Hassabis, *Nature* **2021**, *596*, 583–589.
[51] M. Mirdita, K. Schütze, Y. Moriwaki, L. Heo, S. Ovchinnikov, M. Steinegger, *Nat. Methods* **2022**, *19*, 679–682.
[52] S. Perachon, J.-C. Schwartz, P. Sokoloff, *Eur. J. Pharmacol.* **1999**, *366*, 293–300.
[53] S. Kassel, J. S. Schwed, H. Stark, *Eur. Neuropsychopharmacol.* **2015**, *25*, 1480–1499.
[54] T. Patriarchi, J. R. Cho, K. Merten, M. W. Howe, A. Marley, W. H. Xiong, R. W. Folk, G. J. Broussard, R. Liang, M. J. Jang, H. Zhong, D. Dombeck, M. von Zastrow, A. Nimmerjahn, V. Gradinaru, J. T. Williams, L. Tian, *Science* **2018**, *360*, aat4422.
[55] R. Qanbar, M. Bouvier, *Pharmacol. Ther.* **2003**, *97*, 1–33.
[56] F. Lolicato, H. Juhola, A. Zak, P. A. Postila, A. Saukko, S. Rissanen, G. Enkavi, I. Vattulainen, M. Kepczynski, T. Róg, *ACS Chem. Neurosci.* **2020**, *11*, 1914–1924.
[57] M. Pilla, S. Perachon, F. Sautel, F. Garrido, A. Mann, C. G. Wermuth, J.-C. Schwartz, B. J. Everitt, P. Sokoloff, *Nature* **1999**, *400*, 371–375.
[58] A. E. Moritz, R. B. Free, W. S. Weiner, E. O. Akano, D. Gandhi, A. Abramyan, T. M. Keck, M. Ferrer, X. Hu, N. Southall, J. Steiner, J. Aubé, L. Shi, K. J. Frankowski, D. R. Sibley, *J. Med. Chem.* **2020**, *63*, 5526–5567.
[59] E. S. Gogarnoiu, C. D. Vogt, J. Sanchez, A. Bonifazi, E. Saab, A. B. Shaik, O. Soler-Cedeño, G.-H. Bi, B. Klein, Z.-X. Xi, J. R. Lane, A. H. Newman, *J. Med. Chem.* **2023**, *66*, 1809–1834.
[60] G. Di Giovanni, E. Esposito, V. Di Matteo, *CNS Neurosci. Therap.* **2010**, *16*, 179–194.
[61] F. Lanau, M. T. Zenner, O. Civelli, D. S. Hartman, *J. Neurochem.* **1997**, *68*, 804–812.
[62] M. Sánchez-Soto, A. Bonifazi, N. S. Cai, M. P. Ellenberger, A. H. Newman, S. Ferré, H. Yano, *Mol. Pharmacol.* **2016**, *89*, 457–466.
[63] J. H. Kim, S.-R. Lee, L.-H. Li, H.-J. Park, J.-H. Park, K. Y. Lee, M.-K. Kim, B. A. Shin, S.-Y. Choi, *PLoS One* **2011**, *6*, e18556.
[64] R. K. Sunahara, H.-C. Guan, B. F. O'Dowd, P. Seeman, L. G. Laurier, G. Ng, S. R. George, J. Torchia, H. H. M. Van Tol, H. B. Niznik, *Nature* **1991**, *350*, 614–619.
[65] A. Newman-Tancredi, V. Audinot-Bouchez, A. Gobert, M. J. Millan, *Eur. J. Pharmacol.* **1997**, *319*, 379–383.
[66] N. A. Marze, S. S. Roy Burman, W. Sheffler, J. J. Gray, *Bioinformatics* **2018**, *34*, 3461–3469.
[67] P. B. Stranges, B. Kuhlman, *Protein Sci.* **2013**, *22*, 74–82.
[68] J. Shen, L. Geng, X. Li, C. Emery, K. Kroning, G. Shingles, K. Lee, M. Heyden, P. Li, W. Wang, *Nat. Methods* **2023**, *20*, 112–122.

Manuscript received: May 21, 2025
Accepted manuscript online: June 10, 2025
Version of record online: June 18, 2025

© 2025 The Author(s). Angewandte Chemie International Edition published by Wiley-VCH GmbH